Intensity Interference in a Coherent Spin-Polarized Electron Beam

Makoto Kuwahara,[1,2,*] Yuya Yoshida,[2] Wataru Nagata,[2] Kojiro Nakakura,[2] Masato Furui,[2] Takafumi Ishida,[1,2] Koh Saitoh,[1,2] Toru Ujihara,[1,2] and Nobuo Tanaka[1,3]

[1]*Institute of Materials and Systems for Sustainability, Nagoya University, Nagoya 464-8601, Japan*
[2]*Graduate School of Engineering, Nagoya University, Nagoya 464-8603, Japan*
[3]*Japan Fine Ceramics Center, Nagoya 456-8587, Japan*

(Received 14 December 2020; revised 16 February 2021; accepted 25 February 2021; published 26 March 2021)

We investigate the intensity interference between pairs of electrons using a spin-polarized electron beam having a high polarization and a narrow energy width. We observe spin-dependent antibunching on the basis of coincident counts of electron pairs performed with a spin-polarized transmission electron microscope, which could control the spin-polarization without any changes in the electron optics. The experimental results show that the time correlation was only affected by the spin polarization, demonstrating that the antibunching is associated with fermionic statistics. The coherent spin-polarized electron beam facilitates the extraction of intrinsic quantum interference.

DOI: 10.1103/PhysRevLett.126.125501

The generation of coherent electron beams is an important aspect of electron microscopy, which can provide details regarding atomic structures and precise strains in condensed matter and is also vital in the mapping of electromagnetic fields [1–5]. The spatial and temporal coherence of electron wave packets is also important when observing interference effects, as in the case of diffractive imaging and electron holography, due to the requirement for the electron wave function to have a flat wave front. These various techniques based on electron beams have progressed by providing phase information [6,7]. The phase information has, in turn, contributed to investigations of quantum effects in charged particles, such as the Aharonov-Bohm effect, as well as to the visualization of vector and scalar potentials and applications of the orbital angular momentum of electron waves [8–10]. However, the first-order interference associated with electron holography using a single-electron wave cannot clarify quantum effects, because they are by nature inseparable from classical wave effects. Quantum interference effects can be observed in the second-order correlation function of two particles, such as occur in the Hanbury Brown-Twiss effect [11]. In the case of fermion-type intensity interference, the second-order correlation function exhibits an antibunching effect in coincidences during a coherence time. The intensity interference of electrons was previously observed by Kiesel *et al.* using a highly degenerated electron beam [12]. The degeneracy δ_e of an electron beam is defined as the ratio of the actual coherence volume to the cell volume, and this parameter is an important factor of intensity interference. The degeneracy can be written as $\delta_e = h^3 B/4meE_k\delta E_k$, where B, E_k, and δE_k are the brightness, beam energy, and energy spread, respectively [13,14].

The intensity interference between two electrons was previously examined using a cold field-emission electron source that provided its highest brightness as a nonpolarized electron beam. The results of this prior work suggested that the antibunching effect resulted from either quantum interference or space charge effects [12,15]. These experiments of the intensity interference effect associated with charged particles have only been performed using high-brightness electron beams, so as to obtain antibunching conditions as a result of the correlations between pairs of electrons along the temporal axis. High brightness is not essential for the study of interferometry and coherence, but it is important as a means of suppressing instabilities and achieving a high signal-to-noise ratio by reducing the data acquisition time. The temporal (longitudinal) coherence and spatial (transverse) coherence roughly correspond to the energy dispersion and the parallelism of the electron beam, respectively. Additionally, spin, one of the degrees of freedom of an electron, affects the intensity interference via the Pauli exclusion principle.

Spin effects involved in intensity interference can be estimated by determining the probability of parallel spin states in the density matrix of a two-spin system, representing the tensor product of the density matrices of two one-spin systems [16]. The second-order time-correlation function $g^{(2)}(t)$ for two fermions can be written as

$$g^{(2)}(t) \sim 1 - \frac{1}{2}(1 + P^2)g^{(1)}(t), \tag{1}$$

where P and $g^{(1)}(t)$ are the spin polarization of the electron beam and a first-order time-correlation function, respectively. The antibunching term in $g^{(2)}(t)$ depends on the degree of parallelism of two spins.

We have developed spin-polarized transmission electron microscopy (SP-TEM) using a semiconductor photocathode having a negative electron affinity (NEA) surface as a source of spin-polarized electrons [17]. The quantum axis of spin is aligned perpendicular to the photocathode surface due to the quantized microstructure of the photocathode. The spin-polarized electron beam can provide second-order interference with a high degree of contrast as a result of the antibunching effect associated with intensity interference and the Pauli exclusion effect. In such systems, the electron beam is emitted from the flat surface of a GaAs–GaAsP strained superlattice, with a small spot size of 1.8 μm. This emission process provides several advantages, including a narrow energy range and a small transverse momentum, due to the minimal amount of residual energy in the band structure of the semiconductor. The energy distribution of the electron beam produced in the SP-TEM has been shown to have a full width at half maximum value of 114 ± 32 meV, corresponding to a root-mean-square (rms) temporal coherence τ_c of $(9 \pm 2) \times 10^{-14}$ s, which is evaluated by $\tau_c \sim h/\delta E_k$ [12]. The SP-TEM system provides a high degeneracy of 4×10^{-6} at an excitation wavelength of 778 nm, which is the same order of magnitude as that for a cold field-emission source [17]. Moreover, by providing a maximum polarization of 90% and a long coherence time, SP-TEM can enhance the antibunching effect relative to that obtained from the unpolarized electron beam used in Kiesel's experiments [18]. Employing a regularly pulsed electron beam in conjunction with SP-TEM also increases the signal-to-noise ratio by reducing the noise during noncounting intervals [19–21]. The spin-polarized electrons extracted from the semiconductor photocathode having an NEA surface have sufficient coherence to provide first-order interference and are also expected to generate second-order interference because of their high degeneracy.

Figure 1 shows the experimental setup we used for intensity interference measurements based on SP-TEM combined with a pulsed laser system for polarized electron emission. In this system, a pair of single-electron detectors is positioned after a magnifying lens system that adjusts the spatial coherence length at the detector position via expansion of the electron beam. Each of these detectors is capable of counting individual electrons. The spatial coherence at the detector position is measured using an electron imaging sensor and an electron holography unit capable of generating interference fringes based on the superposition of electron waves. The dual single-electron detector system comprises multichannel plates (MCPs) and two detection electrodes connected to a fast-timing preamplifier (ORTEC, model VT120) and a timing filter amplifier (Canberra, model 2111). The two amplified pulse signals from this unit are sent to a time-to-amplitude converter (Canberra, model 2145) and a multichannel analyzer (MCA) (Canberra, Multiport II) to determine

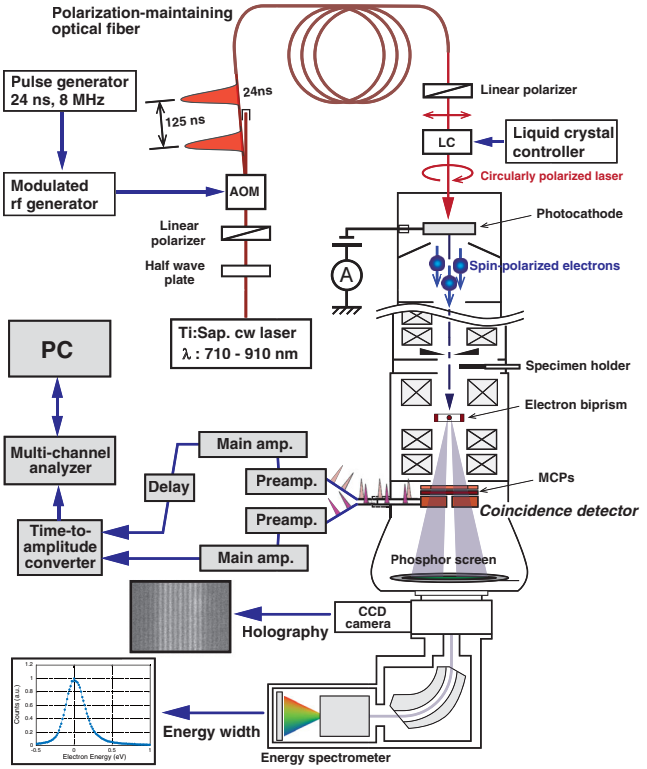

FIG. 1. Experimental setup for detecting the coincidence of two electrons in conjunction with the SP-TEM. The setup comprises a temporally modulated laser controlled by an acoustic optical modulator (AOM), a liquid crystal (LC) controller, and several wave plates generate spin-polarized electrons with variable polarization and temporal structures. The SP-TEM incorporates an electron biprism to create an interference fringe and separate the coherent electron beam into two positions. A pair of single-electron detectors for coincidence counting are constructed from MCPs and two collectors. These detectors are mechanically retractable to allow observation of the interference fringe created by the electron biprism using a phosphor screen and CCD camera.

the time delay between the two electrons. This time-correlation system has a resolution of 48 ps, except for the MCPs. This resolution was confirmed by inputting two artificial pulses into the amplifier circuits. Coincidence counting is performed with a dead time τ_{dead} of 7 μs in each counting event. The bias voltages of the MCPs are set to be -1.5 and -0.5 kV with consideration of the balance between the dark counts and the gain.

The spin polarization of the electron beam generated in the SP-TEM system is controlled by the circular polarization of the drive laser. The sign of the polarization corresponds to the parallel direction to the wave vector of the electron beam. In this system, positive and negative polarizations are obtained via the left- and right-handed circular polarization of the drive laser, respectively, while a nonpolarized condition is achieved using a linearly polarized laser. The time structure of the spin-polarized electron beam is modulated to obtain a bunch width σ_e of 8 ns in rms

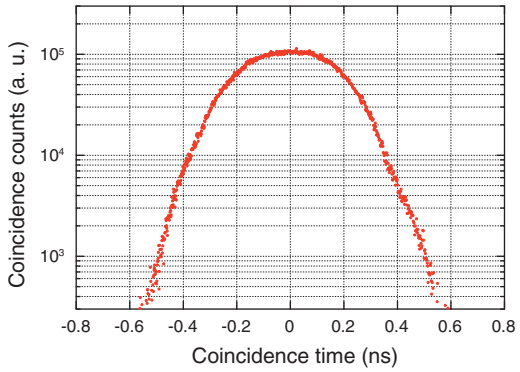

FIG. 2. Coincidence counts of nonpolarized electrons for a counting time of 7.2×10^3 s as a function of the coincidence time.

at a repetition rate f_e of 8 MHz, which suppresses the pileup of pulse signals in the circuit. The spatial coherence length in this system was expanded to approximately 15 mm, which exceeded the detector size, while the electron charge was adjusted to a value of 10^6 electrons per bunch at the electron gun to suppress the Boersch effect by observing the energy width using a spectrometer placed under the imaging detectors [19]. The coherence length l_c can typically be calculated as $\lambda/2\Theta$, where λ and Θ are the wavelength of the electron beam and the parallelism, respectively [22]. The initial emittance was approximately 3×10^{-9} m rad at a beam energy of 30 keV [23]. The coherent current was evaluated to be $6 \times 10^{-4}\%$ of the initial emission current based on the initial emittance and the parallelism value, which provided an effective number of electrons at the detector position of approximately six electrons per bunch, as determined by monitoring the source current of 1.3 μA and the laser spot size on the photocathode [17].

The time correlation between two electrons in a bunched beam was ascertained using the single-electron detector pair and the coincidence measurement system. We carried out three series of measurements using positively polarized, nonpolarized, and negatively polarized electron beams to investigate the origin of the difference between the experimental data and ideal coincidence function. These measurements were conducted 36 times with an acquisition time of 7.2×10^3 s for each spin polarization. This series of measurements was performed 11 times. During these experiments, the polarization values of the electron beams were changed to $+83\%$, 0%, and -80% by controlling the optical circular polarization with an excitation wavelength of 770 nm, so as to obtain high quantum efficiency and generate an electron beam with high charge density [18].

Figure 2 shows the coincidence count using nonpolarized electrons in a counting time of 7.2×10^3 s as a function of coincidence time. The detecting system has a window of about 1 ns to obtain effective counting numbers and to reduce the detection rate at the MCA. The total

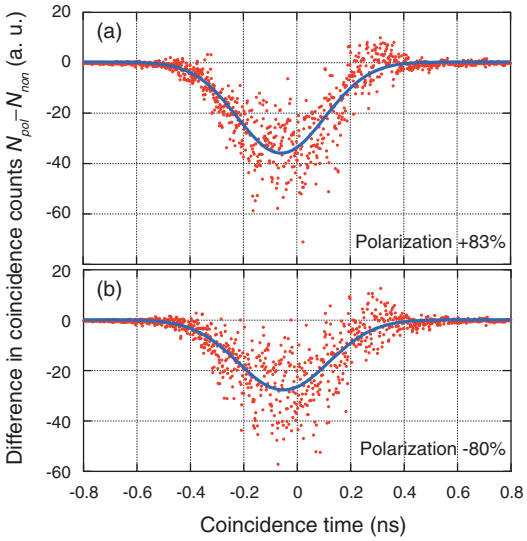

FIG. 3. Differences between the mean coincidence counts of polarized electrons N_{pol} and nonpolarized electrons N_{non} in 7.2×10^3 s as a function of the coincidence time for (a) positive and (b) negative polarizations. Red dots and blue lines indicate data points and fitting curves, respectively.

coincidence count was 3.5×10^7. The measured counting rate $\bar{n}$ was 4.8×10^3 counts/s, which was low in comparison with $1/\tau_{\mathrm{dead}}$. The probability of count loss was estimated to be 3% for a nonparalyzable dead time [24]. The low count loss ($\bar{n}\tau_{\mathrm{dead}} \ll 1$) does not affect the statistics of the measured coincidence count.

Figure 3(a) shows the differences in the coincidence numbers between the positively polarized counts N_{pol} and the nonpolarized counts N_{non}. The red dots show experimental data for each coincidence time of 1.4 ± 0.1 ps/channel. The coincidence events in conjunction with the polarized condition were evidently reduced by a spin effect, in accordance with Eq. (1). Here, the blue solid line is a fitting curve based on a Gaussian function. The negative polarization data are shown in Fig. 3(b) and demonstrate a similar reduction in the coincidence.

The contribution of the polarization to the antibunching effect was analyzed by conducting a fitting analysis using the Gaussian function $I_s \exp(-t^2/2\tau_s^2)$, where I_s and τ_s are the correlation amplitude and temporal width of the subtraction data, respectively. The fitting results are provided in Table I. There are clear differences between the polarized and nonpolarized coincidences, which exceed the margins of error in both cases. It is also evident that the values of the positive and negative polarization data were of the same order of magnitude, suggesting the reliability of the experimental setup incorporating fixed electron optics.

The difference data demonstrate an intrinsic quantum effect on the intensity interference with a value of $-P^2 g^{(1)}(t)/2$. However, the antibunching amplitude was too small compared with the ideal spin dependence. Considering the convolution of the intrinsic interference

TABLE I. Summary of the spin dependence results for the antibunching effect.

Parameter	Polarization +83%	Polarization −80%
Amplitude I_s (channel^{-1})	-37 ± 2	-28 ± 2
Width τ_s (ps)	165 ± 7	171 ± 9
$\lvert I_s/N_{\mathrm{non}}\rvert$	$(3.4 \pm 0.2) \times 10^{-4}$	$(2.6 \pm 0.2) \times 10^{-4}$
$\frac{1}{2}P^2\tau_c/\tau_s$	$(2.3 \pm 0.9) \times 10^{-4}$	$(2.0 \pm 0.7) \times 10^{-4}$
$\sum_{t=-\tau_s/2}^{\tau_s/2}(N_{\mathrm{pol}} - N_{\mathrm{non}})$	-4.2×10^3	-3.6×10^3
$\sum_{t=-\tau_s/2}^{\tau_s/2}(N_{\mathrm{pol}} - N_{\mathrm{non}})/\sum_{t=-\tau_s/2}^{\tau_s/2} N_{\mathrm{non}}$	-3.2×10^{-4}	-2.6×10^{-4}

function and the temporal resolution of the detection system, the fitting function $0.5P^2 \int g^{(1)}(t-t') \cdot \exp(-t'^2/2\tau_d^2)dt'$ was obtained, where τ_d is the temporal resolution of the detector. If a Gaussian first-order interference function is employed, this function can be rewritten as $0.5P^2(\tau_c/\tau_d)\exp[-t^2/2(\tau_d^2+\tau_c^2)]$. Therefore, the width of $\sqrt{\tau_d^2+\tau_c^2}$ is an observed antibunching width τ_s. Table I also presents the $0.5P^2\tau_c/\tau_s$ values and the relative decreases in the coincidence values, with reductions for positive and negative polarizations of 2.3×10^{-4} and 2.0×10^{-4}, respectively. The experimentally determined spin-dependent part of the antibunching effect $|I_s/N_{\mathrm{non}}|$ obtained in the present Letter agrees with the expected value based on the characteristics of the spin-polarized electron beam and the temporal resolution of the detection system for both the positive and negative polarizations.

The summations of difference data in the time range of τ_s are shown in Table I. These summation results also reveal the existence of the antibunching effect with both positive and negative polarization. The summation of coincidence counts in τ_s was 1.3×10^7 in 7.2×10^3 s. The measured counting rate in a bunch was 2.3×10^{-4} counts per bunch, corresponding to a counting rate n_b of 1.3×10^6 counts/s, which is calculated by $n_b = \bar{n}/f_e\tau_s$. In contrast, the counting rate n_b should be estimated by an electron beam density, which is written as $n_b = \int_{-\tau_s/2}^{\tau_s/2}\{(N_e/2)(\eta/\sqrt{2\pi}\sigma_e)\exp(-t^2/2\sigma_e^2)\}^2 dt$, where N_e and η are the number of electrons in a bunch and detection efficiency in the MCP, respectively. The relation $\tau_s \ll \sigma_e$ is used to rewrite the previous expression as $N_e^2\eta^2\tau_s/8\pi\sigma_e^2$. Using the observed counting rate, the expected detection efficiency is estimated to be 0.6, which is reasonable as reported in [25].

In this Letter, we succeeded in observing spin-dependent intensity interference and extracting the intrinsic quantum effect resulting from fermionic statistics. An electron beam with a high polarization, which is a controllable parameter in the SP-TEM apparatus, is evidently a powerful tool for the measurement of quantum interference. The electron microscope system described herein was also able to control the spatial coherence such that it could be adjusted to match the target area. The NEA photocathode simultaneously provided both high brightness and a narrow energy width, meaning that highly degenerate electron wave packets were obtained, which in turn enhanced the intensity interference. Spin-dependent intensity interference experiments were performed without any changes in the electron optics and coherence length and provided evidence for an intrinsic quantum effect associated with charged fermions. To date, the antibunching effect of charged particles has been observed in nonpolarized electron beams emitted from cold field-emission gun systems. However, the results of such measurements could not conclusively indicate whether the intensity interference effect between pairs of fermions arose due to the space charge effect or the quantum effect [12,15]. The present experimental results clarify this matter. In addition, the coherent spin-polarized electron beam demonstrated in this Letter is expected to allow novel fundamental experiments related to quantum statistics and quantum mechanics based on the Pauli principle [13,26,27]. Moreover, this technique could also be applied in conjunction with pulsed scanning electron microscopy and quantum electron microscopy for experiments that require coherent states and quantum entanglements [28,29].

The authors wish to thank Dr. H. Shinada, Dr. M. Koguchi, and Dr. H. Morishita of the Hitachi Central Research Laboratory and Dr. T. Agemura of Hitachi High-Tech for their helpful support and encouragement. This research was supported by JSPS KAKENHI Grants No. 17H02737, No. 17H01072, and No. 15K13404 and by the JST-Mirai Program, Grant No. JPMJMI18G2, Japan.

*kuwahara@imass.nagoya-u.ac.jp

[1] P. Roingeard, Viral detection by electron microscopy: past, present and future, Biol. Cell **100**, 491 (2008).

[2] S. Iijima, Helical microtubules of graphitic carbon, Nature (London) **354**, 56 (1991).

[3] N. Shibata, T. Seki, G. Sánchez-Santolino, S. D. Findlay, Y. Kohno, T. Matsumoto, R. Ishikawa, and Y. Ikuhara, Electric field imaging of single atoms, Nat. Commun. **8**, 15631 (2017).

[4] T. Tanigaki, T. Akashi, A. Sugawara, K. Miura, J. Hayakawa, K. Niitsu, T. Sato, X. Yu, Y. Tomioka, K. Harada, D. Shindo, Y. Tokura, and H. Shinada, Magnetic field obser-

vations in CoFeB/Ta layers with 0.67-nm resolution by electron holography, Sci. Rep. **7**, 16598 (2017).

[5] D. Cooper, N. Bernier, and J. Rouvière, Combining 2 nm Spatial Resolution and 0.02% Precision for Deformation Mapping of Semiconductor Specimens in a Transmission Electron Microscope by Precession Electron Diffraction, Nano Lett. **15**, 5289 (2015).

[6] P. A. Midgley and R. E. Dunin-Borkowski, Electron tomography and holography in materials science, Nat. Mater. **8**, 271 (2009).

[7] J. Yamasaki, S. Morishita, Y. Shimaoka, K. Ohta, and H. Sasaki, Phase imaging and atomic-resolution imaging by electron diffractive imaging, Jpn. J. Appl. Phys. **58**, 120502 (2019).

[8] A. Tonomura, N. Osakabe, T. Matsuda, T. Kawasaki, J. Endo, S. Yano, and H. Yamada, Evidence for Aharonov-Bohm Effect with Magnetic Field Completely Shielded from Electron Wave, Phys. Rev. Lett. **56**, 792 (1986).

[9] M. Uchida and A. Tonomura, Generation of electron beams carrying orbital angular momentum, Nature (London) **464**, 737 (2010).

[10] K. Y. Bliokh, M. R. Dennis, and F. Nori, Relativistic Electron Vortex Beams: Angular Momentum and Spin-Orbit Interaction, Phys. Rev. Lett. **107**, 174802 (2011).

[11] R. Hanbury Brown and R. Q. Twiss, Correlation between photons in two coherent beams of light, Nature (London) **177**, 27 (1956).

[12] H. Kiesel, A Renz, and F. Hasselbach, Observation of Hanbury Brown–Twiss anticorrelations for free electrons, Nature (London) **418**, 392 (2002).

[13] M. P. Silverman, On the feasibility of observing electron antibunching in a field-emission beam, Phys. Lett. A **120**, 442 (1987).

[14] T. Kodama, N. Osakabe, J. Endo, A. Tonomura, K. Ohbayashi, T. Urakami, S. Ohsuka, H. Tsuchiya, Y. Tsuchiya, and Y. Uchikawa, Feasibility of observing two-electron interference, Phys. Rev. A **57**, 2781 (1998).

[15] T. Kodama and N. Osakabe, Mechanism for correlation in a coherent electron beam, Microscopy **68**, 133 (2019).

[16] J. Kessler, *Polarized Electrons*, 2nd ed. (Springer-Verlag, Berlin, Heisenberg, 1985), p. 91–96.

[17] M. Kuwahara, S. Kusunoki, Y. Nambo, K. Saitoh, X. G. Jin, T. Ujihara, H. Asano, Y. Takeda, and N. Tanaka, Coherence of a spin-polarized electron beam emitted from a semiconductor photocathode in a transmission electron microscope, Appl. Phys. Lett. **105**, 193101 (2014).

[18] X. G. Jin, N. Yamamoto, Y. Nakagawa, A. Mano, T. Kato, M. Tanioku, T. Ujihara, Y. Takeda, S. Okumi, M. Yamamoto, T. Nakanishi, T. Saka, H. Horinaka, T. Kato, T. Yasue, and T. Koshikawa, Super-high brightness and high-spin-polarization photocathode, Appl. Phys. Express **1**, 045002 (2008).

[19] M. Kuwahara, Y. Nambo, K. Aoki, K. Sameshima, X. G. Jin, T. Ujihara, H. Asano, K. Saitoh, Y. Takeda, and N. Tanaka, The Boersch effect in a picosecond pulsed electron beam emitted from a semiconductor photocathode, Appl. Phys. Lett. **109**, 013108 (2016).

[20] Y. Nambo, M. Kuwahara, S. Kusunoki, K. Sameshima, K. Saitoh, T. Ujihara, H. Asano, Y. Takeda, and N. Tanaka, Nano-second time-resolved measurement in spin-polarized pulse TEM, AMTC Lett. **4**, 256 (2014).

[21] Y. Honda, S. Matsuba, X. G. Jin, T. Miyajima, M. Yamamoto, T. Uchiyama, M. Kuwahara, and Y. Takeda, Temporal response measurements of GaAs-based photocathodes, Jpn. J. Appl. Phys. **52**, 086401 (2013).

[22] M. Born and E. Wolf, *Principles of Optics*, 7th (expanded) ed. (Cambridge University Press, Cambridge, England, 1999), p. 572.

[23] P. W. Hawkes and H. Kasper, *Principles of Electron Optics* (Academic Press, London, 1989), Vol. 2, Chap. 48.

[24] G. F. Knoll, *Radiation Detection and Measurement*, 4th ed. (Wiley, New York, 2010), Chap. 4.

[25] M. Galanti, R. Gott, and J. F. Renaud, A high resolution, high sensitivity channel plate image intensifier for use in particle spectrographs, Rev. Sci. Instrum. **42**, 1818 (1971).

[26] M. P. Silverman, Second-order temporal and spatial coherence of thermal electrons, Il Nuovo Cimento **99**, 227 (1987).

[27] P. Kwiat, H. Weinfurter, T. Herzog, A. Zeilinger, and M. A. Kasevich, Interaction-Free Measurement, Phys. Rev. Lett. **74**, 4763 (1995).

[28] H. Morishita, T. Ohshima, M. Kuwahara, Y. Ose, and T. Agemura, Resolution improvement of low-voltage scanning electron microscope by bright and monochromatic electron gun using negative electron affinity photocathode, J. Appl. Phys. **127**, 164902 (2020).

[29] P. Kruit, R. G. Hobbs, C. S. Kim, Y. Yang, V. R. Manfrinato, J. Hammer, S. Thomas, P. Weber, B. Klopfer, C. Kohstall, T. Juffmann, M. A. Kasevich, P. Hommelhoff, and K. K. Berggren, Designs for a quantum electron microscope, Ultramicroscopy **164**, 31 (2016).